Palaeogeography, Palaeoclimatology, Palaeoecology 641 (2024) 112136

Contents lists available at ScienceDirect

Palaeogeography, Palaeoclimatology, Palaeoecology

journal homepage: www.elsevier.com/locate/palaeo

Strontium isotope evidence for regional enhanced continental weathering during the early Toarcian in the Tethys Himalaya

Yubo Yang [a], Zhong Han [a,b,*], Xiumian Hu [b], Tianchen He [c], Robert J. Newton [d], Jason Harvey [d]

[a] State Key Laboratory of Oil and Gas Reservoir Geology and Exploitation and Key Laboratory of Deep-time Geography and Environment Reconstruction and Applications, MNR, Institute of Sedimentary Geology, Chengdu University of Technology, Chengdu 610059, China
[b] State Key Laboratory of Mineral Deposit Research, School of Earth Sciences and Engineering, Nanjing University, Nanjing 210023, China
[c] College of Oceanography, Hohai University, Nanjing 210024, China
[d] School of Earth and Environment, University of Leeds, Woodhouse Lane, Leeds LS2 9JT, UK

ARTICLE INFO

Editor: Dr. Bing Shen

Keywords:
Toarcian Oceanic Anoxic Event
Strontium isotopes
Continental weathering
Tibetan Himalaya

ABSTRACT

The early Toarcian of the Early Jurassic was characterized by an interval of global warming, enhanced continental weathering, and an oceanic anoxic event (T-OAE, ~183 Ma). However, the changes in continental weathering intensity in low latitudes still remain poorly constrained. Here, we present strontium isotope ($^{87}Sr/^{86}Sr$) data of the Pliensbachian–Toarcian (Pl–To) interval from the Tibetan Himalaya, which was formerly located in the tropical/subtropical zone of the southeastern Tethys. An abrupt positive shift in $^{87}Sr/^{86}Sr$ starting around the Pl–To boundary and continuing during the interval of the negative carbon-isotope excursion (CIE) suggests enhanced continental weathering and increased terrigenous influx. Stratigraphically higher, the $^{87}Sr/^{86}Sr$ ratios gradually decrease during the recovery phase of the T-OAE CIE, suggesting a decline in continental weathering. Notably, the absolute values and positive-recovery pattern of $^{87}Sr/^{86}Sr$ data from bulk carbonate (pure micrite) of this study are not consistent with that from belemnites and brachiopods of Europe. Based on strong relationship between $^{87}Sr/^{86}Sr$ and diagenetic and silicate-derived Sr proxies, the absolute $^{87}Sr/^{86}Sr$ values here could have been affected to some extent by diagenesis and regional terrestrial input, and thus greatly amplified relative to those of Europe. However, the strontium-isotope positive-recovery pattern broadly corresponds with the pattern and interpretation of other weathering proxies ($\delta^{44/40}Ca$ and $^{187}Os/^{188}Os$) during the T-OAE. These observations suggest that the $^{87}Sr/^{86}Sr$ trend still likely reflects the real regional signal but was superimposed by global influence, although the data were biased by diagenesis. Taken together, the $^{87}Sr/^{86}Sr$ records from Tibetan Himalaya probably provide a useful insight into the regional weathering response, superimposed by the global weathering signal, to the events of the early Toarcian.

1. Introduction

One of the most well-known Oceanic Anoxic Events (OAEs) occurred in the early Toarcian (~183 Ma) and was characterized by the global distribution of contemporaneous organic-rich sediments from both epicontinental and pelagic settings (Jenkyns, 1988; Jenkyns, 2010; Hu et al., 2020; Kemp et al., 2022; Chen et al., 2023). The T-OAE was a profound environmental perturbation of arguably global extent that resulted in disruptions to element cycles, for example, by a sudden negative carbon-isotope excursion (*n*CIE) interrupting a long-term positive CIE (Jenkyns, 2010; Xu et al., 2018; Chen et al., 2021). The T-OAE *n*CIE is believed to be associated with rapid, large-scale CO_2 release from the Karoo-Ferrar Large Igneous Province (LIP), methane hydrate of continental margins or terrestrial environments of wetlands, soils, and lakes (Hesselbo and Jenkyns, 1998; Hesselbo et al., 2000, 2007; Pálfy and Smith, 2000; Them II et al., 2017). Thus, large-scale changes in climate and environmental perturbations were triggered, such as accelerated global warming (Dera et al., 2010; Korte et al., 2015), significant sea-level rise (Hallam, 1981; Haq, 2018), enhanced continental weathering (Brazier et al., 2015; Percival et al., 2016; Kemp et al., 2020), ocean acidification (Müller et al., 2020), and biotic crisis (Harries and Little, 1999; Caswell and Coe, 2014; Jiang et al., 2020).

During the OAEs, enhanced continental weathering could have played a central role in the drawdown of excess atmospheric CO_2 in two

* Corresponding author at: State Key Laboratory of Oil and Gas Reservoir Geology and Exploitation and Key Laboratory of Deep-time Geography and Environment Reconstruction and Applications, MNR, Institute of Sedimentary Geology, Chengdu University of Technology, Chengdu 610059, China.
E-mail address: hanzhong19@cdut.edu.cn (Z. Han).

https://doi.org/10.1016/j.palaeo.2024.112136
Received 26 January 2024; Received in revised form 3 March 2024; Accepted 6 March 2024
Available online 13 March 2024

ways (Jenkyns, 1988, 2010; Hu et al., 2020): (1) chemical weathering consuming CO_2 directly and/or (2) increased continental weathering and nutrient input promoting primary productivity and large-scale burial of organic matter. Although the obvious increase in chemical weathering and associated nutrient delivery have been widely recognized by strontium- osmium- and calcium-isotope data (Cohen et al., 2004; Brazier et al., 2015; Percival et al., 2016; Kemp et al., 2020), strontium-isotope data still remain the persistent positive values after the T-OAE CIE. To date, these continental weathering proxies are all from the northern hemisphere and similar research has been undertaken on southern hemisphere material by using carbonate-hosted water-insoluble elements (e.g., Al, Ti, Sc, Th and total rare earth elements (REE); Han et al., 2022b). However, these continental weathering proxies are not completely coupled, probably due to the partial contribution of authigenic phases (Al) or release (REE) during Fe—Mn oxides dissolution (Han et al., 2022b). Thus, these uncertainties limit our understanding of the changes in global continental weathering.

Here, we present $^{87}Sr/^{86}Sr$ data of carbonate rocks from the Nianduo section (Tethys Himalaya) during the Pl–To interval, previously investigated by Han et al. (2016, 2018), Han et al., 2021, 2022a, 2022b), to constrain changes in continental weathering and provide a better understanding of the strontium-isotope cycle.

2. Geological setting and stratigraphy

The studied area is located in the Tethys Himalaya, Tibet, which was situated in the mature passive margin of the southeastern Neotethys during the Early Jurassic. This was close to the equatorial regions of the southern hemisphere, and is now bounded by the Greater Himalaya to the south and by the Yarlung Zangbo Suture Zone to the north (Fig. 1; Liu and Einsele, 1994; Sciunnach and Garzanti, 2012; Huang et al., 2015). The sedimentary sequence of the Tethys Himalaya consists mainly of Proterozoic to Eocene carbonate and siliciclastic rocks, which originally represented the northern margin deposits of the Indian subcontinent (Fig. 1A; Liu and Einsele, 1994; Jadoul et al., 1998; Sciunnach and Garzanti, 2012).

The Nianduo section (28°40′52″N, 86°08′07″E) of the Nyalam area is located on the Kioto Carbonate Platform (Fig. 1B), which has been well studied and subdivided into the Pupuga and Nieniexiongla Formations (Fig. 2; Jadoul et al., 1998; Han et al., 2016, 2018, 2021). The Pupuga Formation is characterized by thick-bedded bioclastic packstones and was deposited on a shallow-water carbonate platform (Han et al., 2016, 2018). Based on the biostratigraphical data of larger benthic foraminifera and *Lithiotis* bivalves, the Pupuga Formation spans the Pliensbachian to earliest Toarcian (Han et al., 2018, 2021). The overlying lower Nieniexiongla Formation is characterized by micrites deposited on a deeper-water carbonate ramp, intercalating with abundant coarse-grained storm-generated beds (Han et al., 2016, 2021). The lower Nieniexiongla Formation is Toarcian to Aalenian, as inferred from Toarcian foraminifera in the basal units and Bajocian ammonites in the upper part (Jadoul et al., 1998; Han et al., 2021, 2022b). Based on the biostratigraphy, the Pupuga–Nieniexiongla transitional interval records the typical characteristics of the T-OAE CIE: Rapid sea-level rise, carbonate platform crisis, frequent tempestite layers, negative carbon-isotope excursion, and a positive carbonate associated sulfur isotope excursion (Newton et al., 2011; Han et al., 2016, 2018, 2021, 2022a, 2022b).

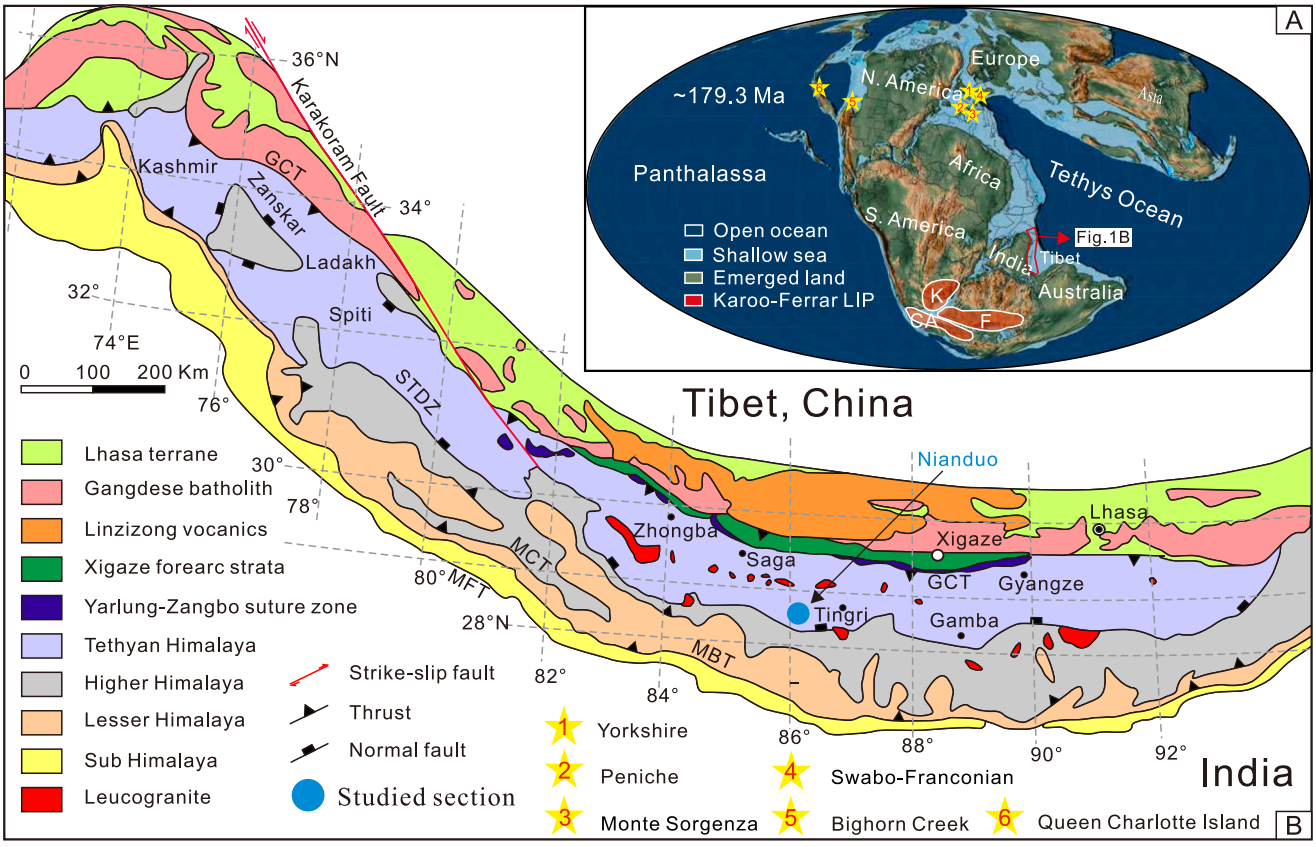

Fig. 1. (A) Toarcian global paleogeographic map (~179.3 Ma, Scotese, 2014) and (B) geological sketch map of the Himalaya showing the studied section, modified after Hu et al. (2016). Abbreviations: GCT: Great Counter Thrust; STDZ: South Tibetan Detachment Zone; MCT: Main Central Thrust; MBT: Main Boundary Thrust; MFT: Main Frontal Thrust. Star 1: Yorkshire, UK; Star 2: Peniche, Portugal; Star 3: Monte Sorgenza, Italy; Star 4: Swabo-Franconian Basin, Germany; Star 5: East Tributary of Bighorn Creek, Canada; Star 6: Queen Charlotte Islands, Canada.

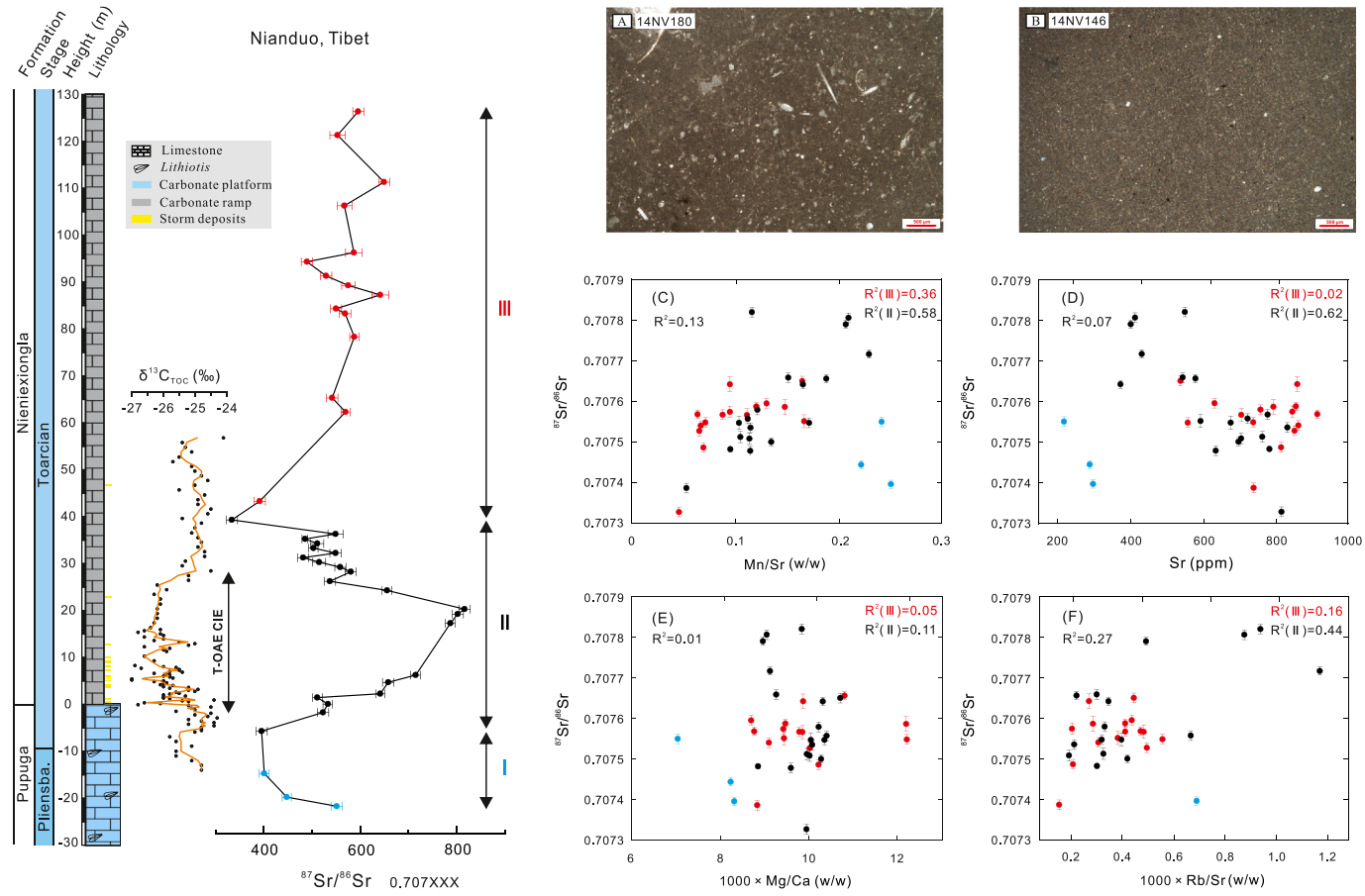

Fig. 2. The carbonate $^{87}Sr/^{86}Sr$ profile of the Nianduo section (this study), photomicrographs of typical micritic limestones (A. 14NV180, −14.6 m; B. 14NV146, 4.8 m) used for strontium-isotope analysis, and evaluation of possible diagenetic and terrestrial input alteration of $^{87}Sr/^{86}Sr$ values. The Sr-isotope profile was divided into pre- (I: −21.6 – −5.6 m), syn- (II: −5.6– 39.4 m), and post- (III: 39.4– 126.4 m) T-OAE CIE intervals. Cross-plots of $^{87}Sr/^{86}Sr$ against elemental concentrations: (C) $^{87}Sr/^{86}Sr$ - Mn/Sr (w/w) ($R^2 = 0.13$), (D) $^{87}Sr/^{86}Sr$ - Sr(ppm) ($R^2 = 0.07$), (E) $^{87}Sr/^{86}Sr$ - 1000 × Ca/Mg(w/w) ($R^2 = 0.01$), and (F) $^{87}Sr/^{86}Sr$ - Rb/Sr (w/w) ($R^2 = 0.27$).

3. Materials and analytical methods

3.1. Sample selection and sequential extraction

Samples were collected from the upper Pupuga–lower Nieniexiongla of the Nianduo section in the southern part of the Tethys Himalaya that spans the T-OAE (Han et al., 2018, 2022b). Thin sections of these samples were first checked to select the best-preserved rock components (pure micrite in this study; Fig. 2A-B) according to the guidelines for the selection of bulk marine carbonate, because this type of carbonate has greater resistance to diagenetic alteration (Bailey et al., 2000; Li et al., 2011; Zhou et al., 2020). Hand samples were cut into fresh rock chips which were then micro-drilled for ~1 g powder within 0.5 cm^2 area, taking care to avoid cement-filled pores, veins and bioclasts. Samples selected by petrographic evaluation were further screened by geological selection criteria (Bailey et al., 2000; Li et al., 2011, 2013; Zhou et al., 2020). After mixing and homogenizing, approximately 50 mg of powder for each sample was reacted with an excess (~3 ml) of 10% (v/v) hydrochloric acid for 24 h at room temperature and this process was accelerated by frequently using an ultrasonic bath. After centrifugation, aliquots of supernatant for each sample were extracted and analyzed for acid-removable Ca, Mg, Al, Sr and Rb, using a Thermo Fisher iCAP 7400 radial Inductively Coupled Plasma Optical Emission Spectrometer (ICP-OES). Analytical uncertainties for these analyses were better than ±5% (RSD).

According to the elemental concentrations from HCl leaching, only samples with [Sr] > 150 ppm, [Rb] < 1 ppm, [Al] < 0.1%, carbonate content >85%, low Mn/Sr ratio (in most cases ≤0.5) and Mg/Ca ratio (in most cases <0.01) were chosen for sequential acid leaching, because these criteria indicate that bulk samples least likely provide secondary seawater $^{87}Sr/^{86}Sr$ values (Bailey et al., 2000; Li et al., 2011; Zhou et al., 2020). The two sequential leaching steps of the dissolution procedure by Li et al. (2011) and He (2017) were employed for 200 mg powders from paired samples of HCl leaching: (1) A calculated volume of diluted acetic acid (0.3 N) was used to dissolve roughly 30% of the carbonate based on the total HCl-leachable carbonate content data, which is designed to remove radiogenic strontium from exchange sites on or within clays and broken mineral surfaces from powdering; (2) After centrifugation and a rinse with ultrapure water (18 MΩ cm^{-1}), the residue was treated using the same procedure to dissolve another 40% of the carbonate, which is expected to represent the near-primary carbonate component. The supernatant of the second acetic acid leachate solution was separated from the residue after centrifugation. An aliquot of this solution was taken to analyze for its elemental concentration. Another aliquot was dried down on a hotplate with a constant temperature of 140 °C, and then re-dissolved using 0.5 ml 3 N HNO_3. This step was repeated three times to fully remove the acetate. The final solution was then dissolved in 0.55 N HNO_3 and passed through a column with Eichrom Sr-Spec resin to purify Sr prior to isotopic determination. All the pre-analysis extraction was performed in the School of Earth and Environment at the University of Leeds.

3.2. Strontium-isotope and elemental concentration measurement

Strontium-isotope analysis was performed by thermal ionization mass spectrometry (TIMS) at the University of Leeds. The Sr isotope ratios and their corresponding standard error (better than 0.000018, 2 s.e.) of the mean are listed in the Appendix. Short-term (about one month) reproducibility was monitored by repeated measurements of NBS-987 ($n = 5$) and was found to be ±0.000004 (1 SD) with an average $^{87}Sr/^{86}Sr$ of 0.710264 which is broadly consistent with the standard value of 0.710248 (McArthur et al., 2012). Within each analytical session, the reported $^{87}Sr/^{86}Sr$ data were corrected by the difference between the measured mean NBS-987 values and the recommended value of 0.710248 (McArthur et al., 2012; typically <0.000018, see more details in the Appendix).

Major and trace element concentrations (Sr, Rb, Al) from the 2nd leachate during sequential leaching were measured using a Thermo Fisher iCAP 7400 radial Inductively Coupled Plasma Optical Emission Spectrometer (ICP-OES) and inductively coupled plasma mass spectrometry (ICP-MS), respectively. Analytical uncertainty for this analysis was <5% (RSD).

4. Results

4.1. Elemental concentrations

The data reported below were obtained from the 2nd leachate after sequential leaching. The Sr concentrations from the carbonate rocks range from 217 to 914 ppm (654 ± 186; 1SD, $n = 36$) for the Nianduo section. The Al concentrations are relatively low, ranging from 62 to 331 ppm (144 ± 60; 1SD, $n = 30$). Carbonate Mn/Sr, Mg/Ca, and Rb/Sr ratios mainly range from 0.04 to 0.25 (0.13 ± 0.06; 1SD, $n = 36$), (7.04 to 12.22) × 10^{-3} ((9.71 ± 0.99) × 10^{-3}; 1SD, $n = 36$), and (0.15 to 1.17) × 10^{-3} ((0.43 ± 0.32) × 10^{-3}; 1SD, $n = 32$), respectively.

4.2. Strontium isotopes

The carbonate $^{87}Sr/^{86}Sr$ profile of the Nianduo section shows an oscillation between 0.707391 and 0.707550 before the Pliensbachian–Toarcian (Pl–To) boundary (~ −21.6 to −5.6 m; Fig. 2), followed by an overall positive excursion and reaching its peak values (~ 0.707821) in the negative interval of the T-OAE CIE (over the interval from −5.6 to 20.4 m; Fig. 2). Following this, $^{87}Sr/^{86}Sr$ starts to decrease and reaches ~0.707513 (~ 21.4 to 31.4 m; Fig. 2) in the recovery interval of the T-OAE CIE. Well after the CIE, $^{87}Sr/^{86}Sr$ achieves relatively stable values between 0.707479 and 0.707548 (~ 31.4 to 36.4 m; Fig. 2). Higher in the section, $^{87}Sr/^{86}Sr$ values show large oscillations during the interval of ~36.4 to 62.4 m with limited datapoints and subsequently maintain relatively stable values between 0.707487 and 0.707651 (Fig. 2).

5. Discussion

5.1. Diagenetic evaluation of strontium isotopes

To establish high-resolution global chemical stratigraphic correlation profiles and reconstruct paleoenvironment changes, the contributions of diagenesis, regional and global seawater to the $^{87}Sr/^{86}Sr$ ratios need to be evaluated. Strontium-isotope composition of marine carbonates is susceptible to alteration in burial and meteoric environments (Wierzbowski et al., 2017). Our analyzed samples are dominated by pure micrite, which retained their sedimentary fabrics (micritic to near-micritic texture) (Fig. 2A-B). According to the guidelines for the sample selection of bulk marine carbonate, this type of carbonate has greater resistance to diagenetic alteration, and is least likely to yield a secondary signal (Li et al., 2011).

Although the $^{87}Sr/^{86}Sr$ ratio of marine carbonates, especially micrites, is widely regarded as a reliable proxy for primary seawater composition (Veizer et al., 1999; Bellefroid et al., 2018), some studies have pointed out that diagenetic alteration and dolomitization can cause significant alteration in $^{87}Sr/^{86}Sr$ (Veizer, 1983; Marshall, 1992; Bellefroid et al., 2018). During the sediment burial history, typical chemical features of carbonates that have undergone a high degree of diagenetic alteration are high Mn/Sr ratios, high $^{87}Sr/^{86}Sr$ ratios, and low Sr values (Veizer, 1983; Kaufman et al., 1993; Derry et al., 1994). Therefore, bivariate plots of Mn/Sr ratios, Sr values and $^{87}Sr/^{86}Sr$ ratios can be an effective way to evaluate the degree of diagenetic alteration. Although the $^{87}Sr/^{86}Sr$ values of the whole section exhibit a poor correlation with Mn/Sr ratios ($R^2 = 0.13$, $n = 36$; Fig. 2C) and Sr concentrations ($R^2 = 0.07$, $n = 17$; Fig. 2D), they show a strong correlation with Mn/Sr ($R^2 = 0.58$, $n = 21$; Fig. 2C), and Sr concentrations ($R^2 = 0.62$, $n = 17$; Fig. 2D) in the interval from ~−5.6 to 39.4 m, suggesting that the $^{87}Sr/^{86}Sr$ values were affected some extent by diagenetic alteration. The potential effect of dolomitization was tested by plotting Mg/Ca ratios against $^{87}Sr/^{86}Sr$ ratios. The measured Mg/Ca ratios (< 0.01) in the Nianduo, coupled with the absence of any correlation with $^{87}Sr/^{86}Sr$ ($R^2 = 0.01$, $n = 36$; Fig. 2E), suggest that dolomitization had a negligible effect on $^{87}Sr/^{86}Sr$ in this study. These observations suggest that samples approximately coincident with the nCIE interval of the Nianduo section were affected some extent by diagenesis, and thus the $^{87}Sr/^{86}Sr$ signal is overprinted in this interval.

5.2. Other possible triggers of the $^{87}Sr/^{86}Sr$ record changes

The early Toarcian was characterized by large-scale changes in global climate and environment associated with emplacement of the Karoo-Ferrar LIP (Burgess et al., 2015; Percival et al., 2015). Therefore, it is possible that the changes in sea-level, volcanic activity of the Karoo-Ferrar LIP, and continental weathering may have driven the evolution of seawater $^{87}Sr/^{86}Sr$. These issues are discussed one by one to constrain the factors that controlled the composition and evolution of $^{87}Sr/^{86}Sr$ in seawater during the early Toarcian of the Tethys Himalaya.

5.2.1. Sea-level changes

Generally, the rise and fall of sea level can cause variations in seawater $^{87}Sr/^{86}Sr$ values. A sea-level transgression can lead to the total land surface shrinking, resulting in the decline of the input of terrigenous strontium, which in turn contributes to a reduction in seawater $^{87}Sr/^{86}Sr$ values (Kani et al., 2013; Wang et al., 2018). Regression causes the opposite effect. Thus, seawater $^{87}Sr/^{86}Sr$ values are negatively correlated with sea-level change (Burke et al., 1982; Krishnaswami et al., 1992; McArthur et al., 2012).

On the basis of biostratigraphy and the characteristic early Toarcian organic carbon-isotope profile of the Nianduo section, the $^{87}Sr/^{86}Sr$ started to rise at ~−5.6 m around the Pl–To boundary, reaching a maximum value of 0.707821 (~ 20.4 m) near the start of the recovery of the T-OAE CIE. The reconstructed global sea-level changes show that the Pl–To boundary was accompanied by an ephemeral transgressive pulse, followed by a major amplitude and short duration of forced regression in the earliest Toarcian (Fig. 3; Krencker et al., 2019; Ruebsam et al., 2019; Bodin et al., 2023). However, there are no obvious sea-level changes over the Pl–To boundary based on the analysis of carbonate microfacies in the Tethys Himalaya (Fig. 3; Han et al., 2016). Importantly, the changes in $^{87}Sr/^{86}Sr$ are not synchronous with the transgressive–regressive cycle. During the onset interval of the T-OAE CIE, there was a globally recognized large sea-level transgression (Hallam, 1981; Haq, 2018; Ruebsam et al., 2019), which was also observed in the Tethys Himalaya (Fig. 3; Han et al., 2016). However, this large transgression is positively correlated with the rapid increase in seawater $^{87}Sr/^{86}Sr$ ratios. The same relationship was also observed in Europe (Yorkshire and Peniche section; McArthur et al., 2000, 2020). Although the short-term sea-level change would have controlled exposed land area and thus terrigenous strontium input that could have modified the

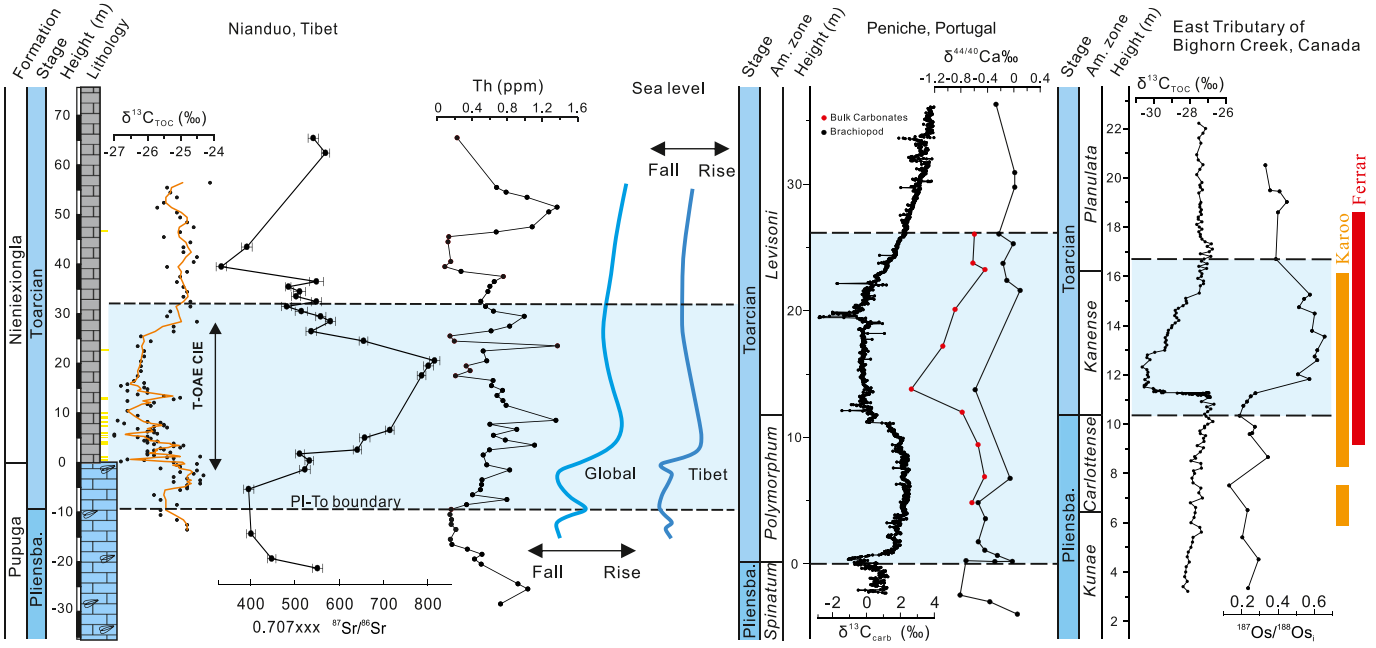

Fig. 3. Systematic variations in geochemical profiles, sea level and magmatic events during upper Pliensbachian–lower Toarcian interval. $\delta^{13}C_{TOC}$ data are from Han et al. (2018), $^{87}Sr/^{86}Sr$ data from this study, Th from Han et al. (2022b), $\delta^{44/40}Ca$ data from Brazier et al. (2015), $^{187}Os/^{188}Os$ data from Them et al. (2017). Sea-level changes of global and Tibet are modified from the compiled data of Ruebsam et al. (2019) and Han et al. (2016), respectively, and phases of the Early Jurassic Karoo-Ferrar volcanism modified from Percival et al. (2015).

$^{87}Sr/^{86}Sr$ evolution of the early Toarcian seawater, the decoupled relationship suggests the negligible influence of sea-level fluctuations. Therefore, it is likely that other factors are more important in influencing the $^{87}Sr/^{86}Sr$ composition of Tibetan carbonates during the early Toarcian.

5.2.2. *Volcanic activity of the Karoo-Ferrar Large Igneous Province*

The significant environmental and biotic perturbations during the late Pliensbachian to early Toarcian have been linked to the volcanism of the Karoo-Ferrar LIP (Fig. 3; Jourdan et al., 2008; Svensen et al., 2007, 2012; Percival et al., 2015; Moulin et al., 2017). Recent high-precision $^{40}Ar/^{39}Ar$ results further indicated that Karoo-Ferrar magmatism triggered the Pl–To extinction event and contributed to the T-OAE (Ware et al., 2023). Thus, a significant role for Karoo-Ferrar LIP in the evolution of seawater $^{87}Sr/^{86}Sr$ is possible. Since Karoo-Ferrar basalts-derived strontium generally has low $^{87}Sr/^{86}Sr$ values (Su et al., 2023), the weathering input from the basalts tend to decrease the $^{87}Sr/^{86}Sr$ ratios in seawater. By contrast, the seawater $^{87}Sr/^{86}Sr$ of Nianduo records an overall gradual positive shift (from 0.707391 to 0.707821) during the negative phase of the T-OAE CIE. This observation does not support the hypothesis that Karoo-Ferrar basalts-derived strontium with low $^{87}Sr/^{86}Sr$ values severely affected the early Toarcian seawater in Sr-isotope compositions. The inference is consistent with the fact that the Karoo-Ferrar LIP occurred on land in temperate regions and thus probably had less impact directly on the seawater $^{87}Sr/^{86}Sr$ compositions.

5.2.3. *Enhanced continental weathering*

Many authors have suggested a link between the Karoo-Ferrar LIP and the perturbed carbon cycle during the T-OAE (e.g., Pálfy and Smith, 2000; Hesselbo et al., 2000; Svensen et al., 2012), which led to increased pCO_2 levels and greenhouse gas-induced global warming. The significant global warming starting around the Pl–To boundary time and reaching maximum temperatures during the negative phase of the T-OAE CIE (Dera et al., 2011; Korte et al., 2015; Müller et al., 2020; Ruebsam et al., 2020). Additionally, an abundance of storm deposits has been discovered at a range of low latitude sites during the early Toarcian, indicating enhanced tropical cyclones likely caused by Toarcian global warming (Krencker et al., 2015; Han et al., 2018), which could have carried elevated rainfall within the tropical cyclone track. Rising temperatures and enhanced rainfall (and thus water availability) would lead to increased terrigenous runoff, causing increased dissolution rates, and thus enhancing chemical weathering rates (Kump et al., 2000; Gislason et al., 2009). These processes have been confirmed by records of weathering proxies such as Os and Ca isotopes (Brazier et al., 2015; Them et al., 2017; Kemp et al., 2020) and carbonate-hosted water-insoluble elements (e.g., Th, Sc, and REE; Han et al., 2022b), although the interpretation of the Ca isotope record is ambiguous because the recent Ca isotope data from Portugal can probably be interpreted in multiple ways (Li et al., 2021). Since crust-derived strontium has relatively high $^{87}Sr/^{86}Sr$ values, a high flux of continentally-derived Sr into seawater can increase the $^{87}Sr/^{86}Sr$ ratios. Therefore, the increase in $^{87}Sr/^{86}Sr$ ratios during the T-OAE CIE in the Tethys Himalaya, as well as in European sections, could have been caused by enhanced continental weathering and terrigenous fluxes (Fig. 3). This observation is similar to the other OAEs (e.g., OAE 1a and OAE 2) which recorded pulses of relatively radiogenic strontium that were also attributed to enhanced continental weathering (Jenkyns, 2010), as further confirmed by zinc- and lithium-isotope records (Pogge von Strandmann et al., 2013; Chen et al., 2020). The volcanism of the Karoo-Ferrar LIP was observed to be broadly synchronous with the $^{87}Sr/^{86}Sr$ positive shift in the Nianduo section (Fig. 3), suggesting that the impact of the Karoo–Ferrar basalts weathering with low $^{87}Sr/^{86}Sr$ values was much lower than that of continental weathering influxes with high $^{87}Sr/^{86}Sr$.

During the recovery interval of the T-OAE CIE, the $^{87}Sr/^{86}Sr$ ratios from Nianduo gradually decreased and maintained relatively stable values (~ 0.7075). This decreasing trend is consistent with the weathering proxies of $\delta^{44/40}Ca$ ratios from Peniche and $^{187}Os/^{188}Os$ ratios from East Tributary, Sakuraguchi-dani, Yorkshire, Mochras and Dormettingen (Fig. 3; Brazier et al., 2015; Them et al., 2017; Kemp et al., 2020). These proxies overall exhibit a positive relationship with $\delta^{18}O$ from belemnite, brachiopod, and TEX_{86} during the recovery interval of the T-OAE CIE (cf. Ruebsam et al., 2020 and references therein), likely suggesting that enhanced organic-carbon burial consumed atmospheric CO_2, continued to lower global temperatures, and gradually reduced

continental weathering. In summary, in addition to diagenesis, continental weathering is also likely to be a dominant factor influencing the $^{87}Sr/^{86}Sr$ ratios change of the early Toarcian seawater in the Tethys Himalaya of the southern hemisphere.

5.3. Comparison with other strontium-isotope records in the early Toarcian

$^{87}Sr/^{86}Sr$ ratios can offer a sensitive and reliable monitor for understanding the evolutionary history of the Earth system (Azmy et al., 1999; Veizer et al., 1999; McArthur et al., 2001, 2012; Korte et al., 2003, 2006). The studied location was located in the open Neotethys Ocean and therefore in a different ocean basin far away from previously studied sections in the European shelf (Yorkshire, UK and the Swabo-Franconian Basin, Germany), western Tethys (Peniche, Portugal and Monte Sorgenza, Italy), and eastern Panthalassa (Queen Charlotte Islands, Canada) (Fig. 1A). The comparison of $^{87}Sr/^{86}Sr$ records at different regions during the Toarcian is beneficial for our understanding of the global $^{87}Sr/^{86}Sr$ evolution in seawater. The $^{87}Sr/^{86}Sr$ data from Tibet are intriguing: The $^{87}Sr/^{86}Sr$ profile is markedly different from that of other records during the interval from Pl–To boundary to the end of the T-OAE CIE in both absolute values and trends (Fig. 4; Gröcke et al., 2007; Woodfine et al., 2008; McArthur et al., 2000, 2020; Frederiksen et al., 2022).

Regarding the differences in absolute values, the absolute $^{87}Sr/^{86}Sr$ values of Tibet (China) are much higher than those of European and Canadian sites during the entire early Toarcian. The main reason is that $^{87}Sr/^{86}Sr$ data of Tibetan Himalaya are partly biased by diagenesis and silicate-derived Sr as discussed in Sections 5.1 and 5.2. Additionally, the studied area was geographically close to the equatorial regions of the southern hemisphere, where the surroundings were probably warmer and wetter than the European sections. Thus, Tibetan Himalaya may have been subjected to stronger continental weathering, which is supported by the Rb/Sr data in this study and carbonate-hosted water-insoluble elements (e.g., Th, Sc, and REE) from the previous study of Han et al. (2022b). The Rb/Sr ratio has been generally used to evaluate the influence of chemical weathering and terrigenous influx, and increases with enhanced chemical weathering (McLennan et al., 1993; Asiedu et al., 2019). This is because Rb^{+} preferentially remains fixed in the weathered residue, but Sr^{2+} is selectively realeased during the continental weathering (Nesbitt et al., 1980). Some correlation is observed between $^{87}Sr/^{86}Sr$ and the Rb/Sr ratio ($R^2 = 0.44$, $n = 17$; Fig. 2F) in the interval between ~−5.6 to 39.4 m, suggesting that the absolute $^{87}Sr/^{86}Sr$ values of Nianduo are partly affected by regional terrestrial inputs. The carbonate-hosted water-insoluble element concentrations are sensitive to the terrigenous influx and can serve as a good monitor for continental chemical weathering (Frimmel, 2009; Zhao and Zheng, 2014; Li et al., 2017). These elements began to increase around the Pl–To boundary and continued to rise during the negative phase of the T-OAE CIE in the Nianduo section (Fig. 3; Han et al., 2022b), which is broadly consistent with the pattern in the strontum isotopes. In conclusion, crust-derived strontium released into the regional seawater through enhanced continental weathering, coupled with effects of post-depositional diagenesis, likely caused higher $^{87}Sr/^{86}Sr$ ratios in the Tibetan Himalaya.

Regarding the differences in trends, the $^{87}Sr/^{86}Sr$ from Nianduo gradually decreased during the recovery interval of the T-OAE CIE, whereas the $^{87}Sr/^{86}Sr$ from the European shelf and western Tethys maintained elevated values after the nCIE (Fig. 4). Notably, the European $^{87}Sr/^{86}Sr$ data are from belemnite and brachiopod calcite, which was thought to be a more true primary seawater signal because these Sr-hosted carbonate materials were not thought to be affected by diagenesis (McArthur et al., 2000, 2020; Frederiksen et al., 2022). Additionally, the $^{87}Sr/^{86}Sr$ trends from several sites (UK, Portugal, Germany, and Italy) in Europe are parallel during this interval (Fig. 4) and thus were logically believed to represent a truly global signal. Thus, the unique $^{87}Sr/^{86}Sr$ trends from the Tibetan Himalaya may have been caused by regional factors, such as local hydrographic restrictions, rates of water renewal, etc., and likely preserve a regional signal. However, it seems to be unsupported by regional and global paleogeographic, environmental, and hydrographic changes, such as the lack of any known geographic barriers between the carbonate platform and southeastern Tethys, comparable fauna assemblages between Tethys Himalaya and western Tethys, significant sea-level rise, or enhanced storm activity during the early Toarcian (Hallam, 1981; Han et al., 2018, 2022a). This evidence for an open setting and free water exchange of the Tethys Himalaya during the early Toarcian suggests that the $^{87}Sr/^{86}Sr$ should theoretically be similar to that, if representing global signal, from Europe, because strontium has a long residence time compared to other elements. Notably, the positive-recovery pattern of $^{87}Sr/^{86}Sr$ of Nianduo from the Tethys Himalaya has a strong similarity to the correlative $\delta^{44/40}Ca$ record from Peniche (western Tethys) and $^{187}Os/^{188}Os$ data from the East Tributary (eastern Panthalassa), Sakuraguchi-dani (eastern Panthalassa), Mochras (UK) and Dormettingen (Germany) from

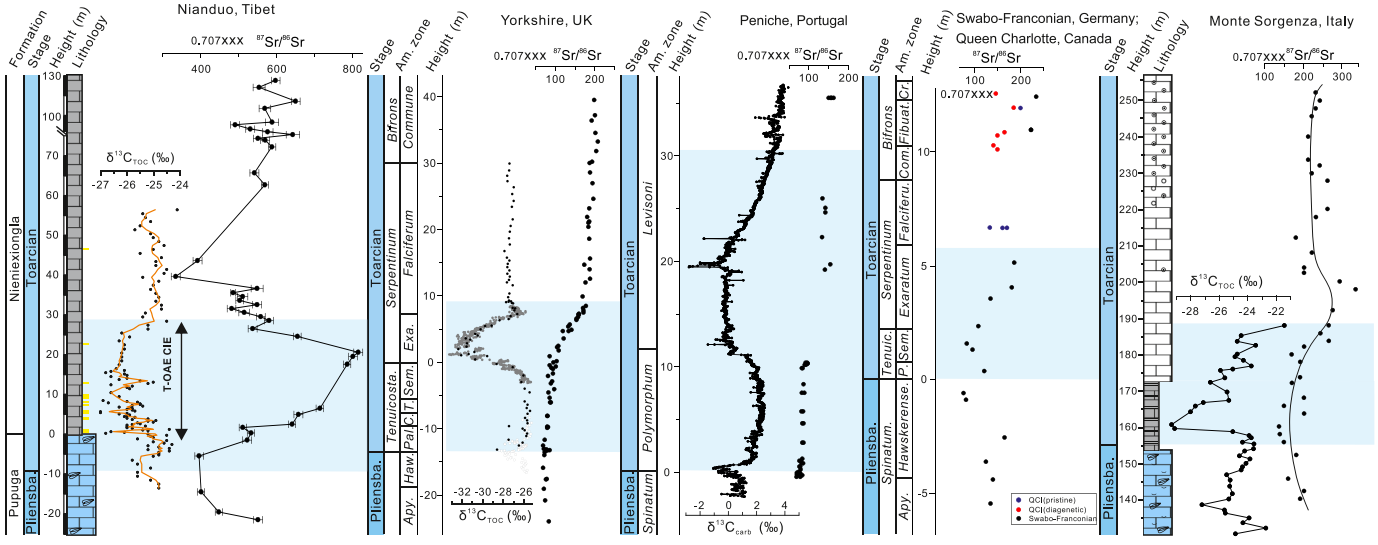

Fig. 4. Comparison of $^{87}Sr/^{86}Sr$ data for the upper Pliensbachian–lower Toarcian interval. For Nianduo section (Tibet), $^{87}Sr/^{86}Sr$ data are from this study. The $^{87}Sr/^{86}Sr$ data of Yorkshire (UK) are from McArthur et al. (2000), of Peniche (Portugal) from McArthur et al. (2020), of Swabo-Franconian Basin (Germany) from Frederiksen et al. (2022), of Queen Charlotte Islands (Canada) from Gröcke et al. (2007), of Monte Sorgenza (Italy) from Woodfine et al. (2008).

northern Europe (Fig. 3; Brazier et al., 2015; Them et al., 2017; Kemp et al., 2020). These observations suggest that although the $^{87}Sr/^{86}Sr$ data from Tibet were affected by diagenetic alternation, its trend likely reflects a real regional signal that was superimposed by a signal of global enhanced continental weathering. In summary, it is hard to reconcile the contradiction between open setting and different $^{87}Sr/^{86}Sr$ evolution from that of Europe. In view of this, we have to reserve the view that the existence of some restriction is still possible because the regional paleogeographic setting for Tibet is less known for Tibet when compared with Europe. Actually, we also could not confirm whether the $^{87}Sr/^{86}Sr$ records from Europe necessarily reflect true global trends, because the persistent positive values after the T-OAE CIE could plausibly be attributed to local hydrographic restriction and rates of water renewal, as confirmed by multiple lines of evidence from isotopes, trace elements and biomarkers (French et al., 2014; Dickson et al., 2017; Them et al., 2017; McArthur et al., 2020; Li et al., 2021; Han et al., 2023).

To date, high-resolution Toarcian strontium-isotope data are still scarce, especially outside of Europe. There are $^{87}Sr/^{86}Sr$ data from Queen Charlotte Islands (Canada), but most of them were affected by diagenesis, and the key T-OAE CIE interval lacks data (Fig. 4; Gröcke et al., 2007). Although the newly reported southern hemisphere $^{87}Sr/^{86}Sr$ data from Tibet are not consistent with those of Europe, they probably provide a useful insight into the regional weathering response, superimposed by the global weathering signal, to the events of the early Toarcian. The exact mechanism driving the discrepancy of $^{87}Sr/^{86}Sr$ between the Tethys Himalaya and Europe still remain equivocal. It is thus necessary to seek additional high-resolution $^{87}Sr/^{86}Sr$ data from other global regions worldwide to confirm the factors that controlled the composition and evolution of seawater $^{87}Sr/^{86}Sr$ during the early Toarcian.

6. Conclusions

This study presents new $^{87}Sr/^{86}Sr$ records of marine carbonate (pure micrite), spanning the Pliensbachian–Toarcian (Pl–To) transitional interval, from the Kioto carbonate platform of the Tethys Himalaya. The absolute values of $^{87}Sr/^{86}Sr$ data in this study were notably higher than those from belemnite and brachiopod calcite of European sites during the entire early Toarcian because our samples were likely biased by diagenesis effects and regional silicate-derived Sr.

An abrupt positive shift of the $^{87}Sr/^{86}Sr$ began around the Pl–To boundary and culminated during the negative phase of the T-OAE CIE, suggesting enhanced continental weathering and increased terrigenous influx that brought more crust-derived strontium to seawater. The $^{87}Sr/^{86}Sr$ gradually decreased during the recovery phase of the T-OAE CIE, illustrating a decline in continental weathering likely due to the CO_2 drawdown caused by organic matter burial. This positive-recovery strontium-isotope pattern corresponds well with the pattern and interpretation commonly used continental weathering proxies from previous investigations. These observations thus suggest that the $^{87}Sr/^{86}Sr$ trend in the Tethys Himalaya likely preserved the real regional signal in continental weathering change, and concurrently superimposed by a signal of global continental weathering, although the data were biased to some degree by diagenesis. Notably, the positive-recovery $^{87}Sr/^{86}Sr$ trend from an open setting of Tibet is not consistent with that from Europe where the belemnite- and brachiopod-derived $^{87}Sr/^{86}Sr$ did not recover but maintained high values after the T-OAE CIE. In general, the driving mechanism for the discrepancy in $^{87}Sr/^{86}Sr$ absolute values and trend between the Tethys Himalaya and Europe is still uncertain, which remains a topic for further research.

CRediT authorship contribution statement

Yubo Yang: Writing – review & editing, Writing – original draft, Formal analysis, Data curation, Conceptualization. **Zhong Han:** Writing – review & editing, Writing – original draft, Supervision, Project administration, Investigation, Funding acquisition, Conceptualization. **Xiumian Hu:** Supervision, Project administration, Funding acquisition. **Tianchen He:** Writing – review & editing, Writing – original draft, Methodology. **Robert J. Newton:** Writing – review & editing, Writing – original draft. **Jason Harvey:** Writing – original draft, Methodology.

Declaration of competing interest

The authors declare that they have no known competing financial interests or personal relationships that could have appeared to influence the work reported in this paper.

Data availability

Data will be made available on request.

Acknowledgements

We thank, Stephen Reid, Crispin Little, Autumn Pugh and Linda Forbes for their help in the laboratory, Xinyang Chen, Wenhan Chen, Shi Sun and Zhongya Hu for their helpful discussion, and constructive suggestions of two anonymous reviewers. This work was supported by the National Natural Science Foundation of China (Nos. 42272116, 41888101 and 42002121) and the Program B (201802B079) for Outstanding PhD student and research grant (2021-LAMD-K03) from the State Key Laboratory of Mineral Deposit Research of Nanjing University. This manuscript is a contribution to the IGCP 739.

Appendix A. Supplementary data

Supplementary data to this article can be found online at https://doi.org/10.1016/j.palaeo.2024.112136.

References

Asiedu, D.K., Agoe, M., Amponsah, P.O., Nude, P.M., Anani, C.Y., 2019. Geochemical constraints on provenance and source area weathering of metasedimentary rocks from the Paleoproterozoic (~2.1 Ga) Wa-Lawra Belt, southeastern margin of the West African Craton. Geodin. Acta 31, 27–39.

Azmy, K., Veizer, J., Wenzel, B., Bassett, M.G., Copper, P., 1999. Silurian strontium isotope stratigraphy. Geol. Soc. Am. Bull. 111, 475–483.

Bailey, T.R., McArthur, J.M., Prince, H., Thirlwall, M.F., 2000. Dissolution methods for strontium isotope stratigraphy: whole rock analysis. Chem. Geol. 167 (3–4), 313–319.

Bellefroid, E.J., Planavsky, N.J., Miller, N.R., Brand, U., Wang, C., 2018. Case studies on the utility of sequential carbonate leaching for radiogenic strontium isotope analysis. Chem. Geol. 497, 88–99.

Bodin, S., Fantasia, A., Krencker, F.-N., Nebsbjerg, B., Christiansen, L., Andrieu, S., 2023. More gaps than record! A new look at the Pliensbachian/Toarcian boundary event guided by coupled chemo-sequence stratigraphy. Palaeogeogr. Palaeoclimatol. Palaeoecol. 610, 111344.

Brazier, J.M., Suan, G., Tacail, T., Simon, L., Martin, J.E., Mattioli, E., Baiter, V., 2015. Calcium isotope evidence for dramatic increase of continental weathering during the Toarcian oceanic anoxic event (Early Jurassic). Earth Planet. Sci. Lett. 411, 164–176.

Burgess, S.D., Bowring, S.A., Fleming, T.H., Elliot, D.H., 2015. High-precision geochronology links the Ferrar large igneous province with early-Jurassic Ocean anoxia and biotic crisis. Earth Planet. Sci. Lett. 415, 90–99.

Burke, W.H., Denison, R.E., Hetherington, E.A., Koepnick, R.B., Nelson, H.F., Otto, J.B., 1982. Variation of seawater $^{87}Sr/^{86}Sr$ throughout Phanerozoic time. Geology 10, 516–519.

Caswell, B.A., Coe, A.L., 2014. The impact of anoxia on pelagic macrofauna during the Toarcian Oceanic Anoxic Event (Early Jurassic). Proc. Geol. Assoc. 125, 383–391.

Chen, X., Sageman, B.B., Yao, H., Liu, S.A., Han, K., Zou, Y., Wang, C., 2020. Zinc isotope evidence for paleoenvironmental changes during cretaceous Oceanic Anoxic Event 2. Geology. 49, 412–416.

Chen, W., Kemp, D.B., He, T., Huang, C., Jin, S., Xiong, Y., Newton, R.J., 2021. First record of the early Toarcian Oceanic Anoxic Event in the Hebrides Basin (UK) and implications for redox and weathering changes. Glob. Planet. Chang. 207, 103685.

Chen, W., Kemp, D.B., He, T., Newton, R.J., Xiong, Y., Jenkyns, H.C., Izumi, K., Cho, T., Huang, C., Poulton, S.W., 2023. Shallow-and deep-ocean Fe cycling and redox evolution across the Pliensbachian–Toarcian boundary and Toarcian Oceanic Anoxic Event in Panthalassa. Earth Planet. Sci. Lett. 602, 117959.

Cohen, A.S., Coe, A.L., Harding, S.M., Schwark, L., 2004. Osmium isotope evidence for the regulation of atmospheric CO_2 by continental weathering. Geology 32, 157–160.

Dera, G., Neige, P., Dommergues, J.-L., Fara, E., Laffont, R., Pellenard, P., 2010. High-resolution dynamics of Early Jurassic marine extinctions: the case of Pliensbachian–Toarcian ammonites (Cephalopoda). J. Geol. Soc. Lond. 167, 21–33.
Dera, G., Brigaud, B., Monna, F., Laffont, R., Puceat, E., Deconinck, J.F., Pellenard, P., Joachimski, M.M., Durlet, C., 2011. Climatic ups and downs in a disturbed Jurassic world. Geology 39, 215–218.
Derry, L., Brasier, M., Corfield, R.E.A., Rozanov, A.Y., Zhuravlev, A.Y., 1994. Sr and C isotopes in lower Cambrian carbonates from the Siberian craton: a paleoenvironmental record during the 'Cambrian explosion'. Earth Planet. Sci. Lett. 128, 671–681.
Dickson, A.J., Gill, B.C., Ruhl, M., Jenkyns, H.C., Porcelli, D., Idiz, E., Lyons, T.W., van den Boorn, S.H.J.M., 2017. Molybdenum-isotope chemostratigraphy and paleoceanography of the Toarcian Oceanic Anoxic Event (Early Jurassic). Paleoceanography 32, 813–829.
Frederiksen, J.A., Ullmann, C.V., Frei, R., Korte, C., 2022. Strontium isotope ratios from the Swabo-Franconian Basin (Germany) and a new compilation of marine $^{87}Sr/^{86}Sr$ signatures for the Upper Sinemurian to Toarcian: global uniformity and driving forces for marine $^{87}Sr/^{86}Sr$. Newsl. Stratigr. 55 (3), 311–331.
French, K.L., Sepulveda, J., Trabucho-Alexandre, J., Grocke, D.R., Summons, R.E., 2014. Organic geochemistry of the early Toarcian oceanic anoxic event in Hawsker Bottoms, Yorkshire, England. Earth Planet. Sci. Lett. 390, 116–127.
Frimmel, H.E., 2009. Trace element distribution in Neoproterozoic carbonates as palaeoenvironmental indicator. Chem. Geol. 258, 338–353.
Gislason, S.R., Oelkers, E.H., Eiriksdottir, E.S., Kardjilov, M.I., Gisladottir, G., Sigfusson, B., Snorrason, A., Elefsen, S., Hardardottir, J., Torssander, P., Oskarsson, N., 2009. Direct evidence of the feedback between climate and weathering. Earth Planet. Sci. Lett. 277, 213–222.
Gröcke, D.R., Hesselbo, S.P., Findlay, D.J., 2007. Atypical diagenetic effects on strontium-isotope composition of early Jurassic belemnites, Queen Charlotte Islands, British Columbia, Canada. Can. J. Earth Sci. 44, 181–197.
Hallam, A., 1981. A revised sea-level curve for the early Jurassic. J. Geol. Soc. 138, 735–743.
Han, Z., Hu, X., Li, J., Garzanti, E., 2016. Jurassic carbonate microfacies and relative sea-level changes in the Tethys Himalaya (southern Tibet). Palaeogeogr. Palaeoclimatol. Palaeoecol. 456, 1–20.
Han, Z., Hu, X., Kemp, D.B., Li, J., 2018. Carbonate-platform response to the Toarcian Oceanic Anoxic Event in the southern hemisphere: implications for climatic change and biotic platform demise. Earth Planet. Sci. Lett. 489, 59–71.
Han, Z., Hu, X., BouDagher-Fadel, M., Jenkyns, H.C., Franceschi, M., 2021. Early Jurassic carbon-isotope perturbations in a shallow water succession from the Tethys Himalaya, southern hemisphere. Newsl. Stratigr. 54, 461–481.
Han, Z., Hu, X., He, T., Newton, R.J., Jenkyns, H.C., Jamieson, R.A., Franceschi, M., 2022a. Early Jurassic long-term oceanic sulfur-cycle perturbations in the Tibetan Himalaya. Earth Planet. Sci. Lett. 578, 117261.
Han, Z., Hu, X., Hu, Z., Jenkyns, H.C., Su, T., 2022b. Geochemical evidence from the Kioto Carbonate Platform (Tibet) reveals enhanced terrigenous input and deoxygenation during the early Toarcian. Glob. Planet. Chang. 215, 103887.
Han, Z., Hu, X., Newton, R.J., He, T., Mills, B.J.W., Jenkyns, H.C., Ruhl, M., Jamieson, R. A., 2023. Spatially heterogenous seawater $\delta^{34}S$ and global cessation of Ca-sulfate burial during the Toarcian oceanic anoxic event. Earth Planet. Sci. Lett. 622, 118404.
Haq, B.U., 2018. Jurassic sea-level variations: a reappraisal. GSA Today 28.
Harries, P.J., Little, C.T., 1999. The early Toarcian (Early Jurassic) and the Cenomanian–Turonian (Late Cretaceous) mass extinctions: similarities and contrasts. Palaeogeogr. Palaeoclimatol. Palaeoecol. 154, 39–66.
He, Tianchen, 2017. Isotopic Constraints on the Palaeoenvironmental Conditions during the Cambrian Radiation of Animals. Doctoral thesis (Ph.D),. University College London.
Hesselbo, S.P., Jenkyns, H.C., 1998. British lower Jurassic sequence stratigraphy. In: de Graciansky, P.-C., Hardenbol, J., Jacquin, T., Vail, P.R. (Eds.), Mesozoic and Cenozoic Sequence Stratigraphy of European Basins, Special Publication Society for Sedimentary Geology (SEPM), vol. 60, pp. 561–581.
Hesselbo, S.P., Gröcke, D.R., Jenkyns, H.C., Bjerrum, C.J., Farrimond, P., Morgans Bell, H.S., Green, O.R., 2000. Massive dissociation of gas hydrate during a Jurassic oceanic anoxic event. Nature 406, 392–395.
Hesselbo, S.P., Jenkyns, H.C., Duarte, L.V., Oliveira, L.C.V., 2007. Carbon-isotope record of the early Jurassic (Toarcian) Oceanic Anoxic Event from fossil wood and marine carbonate (Lusitanian Basin, Portugal). Earth Planet. Sci. Lett. 253, 455–470.
Hu, X., Wang, J., Boudagher-Fadel, M., Garzanti, E., An, W., 2016. New insights into the timing of the India – Asia collision from the Paleogene Quxia and Jialazi formations of the Xigaze forearc basin, South Tibet. Gondwana Res. 32, 76–92.
Hu, X., Li, J., Han, Z., Li, Y., 2020. Two types of hyperthermal events in the Mesozoic–Cenozoic: environmental impacts, biotic effects, and driving mechanisms. Sci. China Earth Sci. 63, 1–18.
Huang, W.T., van Hinsbergen, D.J., Dekkers, M.J., Garzanti, E., Dupont-Nivet, G., Lippert, P.C., Li, X.C., Maffione, M., Langereis, C.G., Hu, X.M., 2015. Paleolatitudes of the Tibetan Himalaya from primary and secondary magnetizations of Jurassic to Lower Cretaceous sedimentary rocks. Geochem. Geophys. Geosyst. 16, 77–100.
Jadoul, F., Berra, F., Garzanti, E., 1998. The Tethys Himalayan passive margin from late Triassic to early cretaceous (South Tibet). J. Asian Earth Sci. 16, 173–194.
Jenkyns, H.C., 1988. The early Toarcian (Jurassic) anoxic event; stratigraphic, sedimentary and geochemical evidence. Am. J. Sci. 288, 101–151.
Jenkyns, H.C., 2010. Geochemistry of oceanic anoxic events. Geochem. Geophys. Geosyst. 11.
Jiang, S., Song, H., Kemp, D.B., Dai, X., Liu, X., 2020. Two pulses of extinction of larger benthic foraminifera during the Pliensbachian–Toarcian and early Toarcian environmental crises. Palaeogeogr. Palaeoclimatol. Palaeoecol. 560, 109998.
Jourdan, F., Feraud, G., Bertrand, H., Watkeys, M.K., Renne, P.R., 2008. The (40)Ar/(39) Ar ages of the sill complex of the Karoo large igneous province: implications for the Pliensbachian-Toarcian climate change. Geochem. Geophys. Geosyst. 9, 1–20.
Kani, T., Hisanabe, C., Isozaki, Y., 2013. The Capitanian (Permian) minimum of $^{87}Sr/^{86}Sr$ ratio in the mid-Panthalassan paleo-atoll carbonates and its demise by the deglaciation and continental doming. Gondwana Res. 24, 212–221.
Kaufman, A.J., Jacobsen, S.B., Knoll, A.H., 1993. The Vendian record of Sr and C isotopic variations in seawater: implications for tectonics and paleoclimate. Earth Planet. Sci. Lett. 120, 409–430.
Kemp, D.B., Selby, D., Izumi, K., 2020. Direct coupling between carbon release and weathering during the Toarcian oceanic anoxic event. Geology 48, 976–980.
Kemp, D.B., Suan, G., Fantasia, A., Jin, S., Chen, W., 2022. Global organic carbon burial during the Toarcian oceanic anoxic event: patterns and controls. Earth Sci. Rev. 231, 104086.
Korte, C., Kozur, H.W., Bruckschen, P., Veizer, J., 2003. Strontium isotope evolution of late Permian and Triassic seawater. Geochim. Cosmochim. Acta 67, 47–62.
Korte, C., Jasper, T., Kozur, H.W., Veizer, J., 2006. $^{87}Sr/^{86}Sr$ record of Permian seawater. Palaeogeogr. Palaeoclimatol. Palaeoecol. 240, 89–107.
Korte, C., Hesselbo, S.P., Ullmann, C.V., Dietl, G., Ruhl, M., Schweigert, G., Thibault, N., 2015. Jurassic climate mode governed by ocean gateway. Nat. Commun. 6, 10015.
Krencker, F.N., Bodin, S., Suan, G., Heimhofer, U., Kabiri, L., Immenhauser, A., 2015. Toarcian extreme warmth led to tropical cyclone intensification. Earth Planet. Sci. Lett. 425, 120–130.
Krencker, F.N., Lindström, S., Bodin, S., 2019. A major sea-level drop briefly precedes the Toarcian oceanic anoxic event: implication for early Jurassic climate and carbon cycle. Sci. Rep. 9, 12518.
Krishnaswami, S., Trivedi, J., Sarin, M., Ramesh, R., Sharma, K.J., 1992. Strontium isotopes and rubidium in the Ganga-Brahmaputra river system: weathering in the Himalaya, fluxes to the Bay of Bengal and contributions to the evolution of oceanic $^{87}Sr/^{86}Sr$. Earth Planet. Sci. Lett. 109, 243–253.
Kump, L.R., Brantley, S.L., Arthur, A., 2000. Chemical weathering, atmospheric CO_2, and climate. Annu. Rev. Earth Planet. Sci. 28, 611–667.
Li, D., Shields-Zhou, G.A., Ling, H.-F., Thirlwall, M., 2011. Dissolution methods for strontium isotope stratigraphy: guidelines for the use of bulk carbonate and phosphorite rocks. Chem. Geol. 290, 133–144.
Li, D., Ling, H.F., Shields-Zhou, G.A., Chen, X., Cremonese, L., Och, L., Thirlwall, M., Manning, C.J., 2013. Carbon and strontium isotope evolution of seawater across the Ediacaran–Cambrian transition: evidence from the Xiaotan section, NE Yunnan, South China. Precambrian Res. 225, 128–147.
Li, W.-P., Zheng, Y.-F., Zhao, Y.-Y., 2017. Geochemical evidence from marine carbonate for enhanced terrigenous input into seawater during the Ediacaran-Cambrian transition in South China. Precambrian Res. 291, 83–97.
Li, Q., McArthur, J.M., Thirlwall, M.F., Turchyn, A.V., Page, K., Bradbury, H.J., Weis, R., Lowry, D., 2021. Testing for ocean acidification during the early Toarcian using $\delta^{44/40}Ca$ and $\delta^{88/86}Sr$. Chem. Geol. 574, 120228.
Liu, G.H., Einsele, G., 1994. Sedimentary history of the Tethyan basin in the Tibetan Himalayas. Geol. Rundsch. 83, 32–61.
Marshall, J.D., 1992. Climatic and oceanographic isotopic signals from the carbonate rock record and their preservation. Geol. Mag. 129, 143–160.
McArthur, J.M., Donovan, D.T., Thirlwall, M.F., Fouke, B.W., Mattey, D., 2000. Strontium isotope profile of the early Toarcian (Jurassic) oceanic anoxic event, the duration of ammonite biozones, and belemnite palaeotemperatures. Earth Planet. Sci. Lett. 179, 269–285.
McArthur, J.M., Howarth, R., Bailey, T.R., 2001. Strontium isotope stratigraphy: LOWESS version 3: best fit to the marine Sr-isotope curve for 0–509 Ma and accompanying look-up table for deriving numerical age. J. Geol. 109, 155–170.
McArthur, J.M., Howarth, R.J., Shields, G.A., 2012. Strontium isotope stratigraphy. In: Gradstein, F.M., Ogg, J.G., Schmitz, M.D., Ogg, G.M. (Eds.), The Geologic Time Scale. Elsevier, Boston, pp. 127–144.
McArthur, J.M., Page, K., Duarte, L.V., Thirlwall, M.F., Li, Q., Weis, R., Comas-Rengifo, M.J., 2020. Sr-isotope stratigraphy ($^{87}Sr/^{86}Sr$) of the lowermost Toarcian of Peniche, Portugal, and its relation to ammonite zonations. Newsl. Stratigr. 53, 297–312.
McLennan, S., Hemming, S., McDaniel, D., Hanson, G.J.S.P.-G.S.o.A, 1993. Geochemical Approaches to Sedimentation, Provenance, and Tectonics, p. 21.
Moulin, M., Fluteau, F., Courtillot, V., Marsh, J., Delpech, G., Quidelleur, X., Gérard, M., 2017. Eruptive history of the Karoo lava flows and their impact on early Jurassic environmental change. J. Geophys. Res. Solid Earth 122, 738–772.
Müller, T., Jurikova, H., Gutjahr, M., Tomašových, A., Schlögl, J., Liebetrau, V., Duarte, L.v., Milovský, R., Suan, G., Mattioli, E., Pittet, B., Eisenhauer, A., 2020. Ocean acidification during the early Toarcian extinction event: evidence from boron isotopes in brachiopods. Geology 48, 1184–1188.
Nesbitt, H.W., Markovics, G., Price, R.C., 1980. Chemical processes affecting alkalis and alkaline earths during continental weathering. Geochim. Cosmochim. Acta 44, 1659–1666.
Newton, R.J., Reeves, E.P., Kafousia, N., Wignall, P.B., Bottrell, S.H., Sha, J.-G., 2011. Low marine sulfate concentrations and the isolation of the European epicontinental sea during the early Jurassic. Geology 39, 7–10.
Pálfy, J., Smith, P.L., 2000. Synchrony between early Jurassic extinction, oceanic anoxic event, and the Karoo-Ferrar flood basalt volcanism. Geology 28, 747–750.
Percival, L.M.E., Witt, M.L.I., Mather, T.A., Hermoso, M., Jenkyns, H.C., Hesselbo, S.P., Al-Suwaidi, A.H., Storm, M.S., Xu, W., Ruhl, M., 2015. Globally enhanced mercury

deposition during the end-Pliensbachian extinction and Toarcian OAE: a link to the Karoo-Ferrar large Igneous Province. Earth Planet. Sci. Lett. 428, 267–280.
Percival, L.M., Cohen, A., Davies, M., Dickson, A., Hesselbo, S., Jenkyns, H., Leng, M., Mather, T., Storm, M., Xu, W., 2016. Osmium isotope evidence for two pulses of increased continental weathering linked to early Jurassic volcanism and climate change. Geology 44, 759–762.
Pogge von Strandmann, P.A.E., Jenkyns, H.C., Woodfine, R.G., 2013. Lithium isotope evidence for enhanced weathering during Oceanic Anoxic Event 2. Nat. Geosci. 6, 668–672.
Ruebsam, W., Mayer, B., Schwark, L., 2019. Cryosphere carbon dynamics control early Toarcian global warming and sea level evolution. Glob. Planet. Chang. 172, 440–453.
Ruebsam, W., Reolid, M., Sabatino, N., Masetti, D., Schwark, L., 2020. Molecular paleothermometry of the early Toarcian climate perturbation. Glob. Planet. Chang. 195, 103351.
Sciunnach, D., Garzanti, E., 2012. Subsidence history of the Tethys Himalaya. Earth Sci. Rev. 111, 179–198.
Scotese, C., 2014. Atlas of Jurassic paleogeographic maps, PALEOMAP Atlas for ArcGIS. In: The Jurassic and Triassic, Maps 32–42. Mollweide Projection, PALEOMAP Project, Evanston, IL, Vol. 4.
Su, Y.-T., Yang, Z.-F., Guo, S.-Y., Li, P.-P., 2023. Contamination of heterogeneous lower crust in Hannuoba tholeiite: evidence from in situ trace elements and strontium isotopes of plagioclase. Am. Mineral. 108, 485–497.
Svensen, H., Planke, S., Chevallier, L., Malthe-Sørenssen, A., Corfu, F., Jamtveit, B., 2007. Hydrothermal venting of greenhouse gases triggering early Jurassic global warming. Earth Planet. Sci. Lett. 256, 554–566.
Svensen, H., Corfu, F., Polteau, S., Hammer, Ø., Planke, S., 2012. Rapid magma emplacement in the Karoo large Igneous Province. Earth Planet. Sci. Lett. 325-326, 1–9.
Them II, T., Gill, B., Caruthers, A., Gröcke, D., Tulsky, E., Martindale, R., Poulton, T., Smith, P., 2017. High-resolution carbon isotope records of the Toarcian Oceanic Anoxic Event (early Jurassic) from North America and implications for the global drivers of the Toarcian carbon cycle. Earth Planet. Sci. Lett. 459, 118–126.
Them, T.R., Gill, B.C., Selby, D., Gröcke, D.R., Friedman, R.M., Owens, J.D., 2017. Evidence for rapid weathering response to climatic warming during the Toarcian Oceanic Anoxic Event. Sci. Rep. 7, 5003.
Veizer, J., 1983. Chemical diagenesis of carbonates: theory and application. In: Stable Isotopes in Sedimentary Geology, Vol. 10, pp. 3–100.
Veizer, J., Ala, D., Azmy, K., Bruckschen, P., Buhl, D., Bruhn, F., Carden, G.A.F., Diener, A., Ebneth, S., Godderis, Y., Jasper, T., Korte, C., Pawellek, F., Podlaha, O.G., Strauss, H., 1999. $^{87}Sr/^{86}Sr$, $\delta^{13}C$ and $\delta^{18}O$ evolution of Phanerozoic seawater. Chem. Geol. 161, 59–88.
Wang, W.Q., Garbelli, C., Zheng, Q.F., Chen, J., Liu, X.C., Wang, W., Shen, S.Z., 2018. Permian Sr-87/Sr-86 chemostratigraphy from carbonate sequences in South China. Palaeogeogr. Palaeoclimatol. Palaeoecol. 500, 84–94.
Ware, B., Jourdan, F., Timms, N.E., 2023. The Ferrar Continental Flood Basalt: a ~1.6 Ma long duration evidenced by high-precision $^{40}Ar/^{39}Ar$ ages suggest a potential role in the Pliensbachian-Toarcian extinction event. Earth Planet. Sci. Lett. 622, 118369.
Wierzbowski, H., Anczkiewicz, R., Pawlak, J., Rogov, M.A., Kuznetsov, A.B., 2017. Revised Middle–Upper Jurassic strontium isotope stratigraphy. Chem. Geol. 466, 239–255.
Woodfine, R.G., Jenkyns, H.C., Sarti, M., Baroncini, F., Violante, C., 2008. The response of two Tethyan carbonate platforms to the early Toarcian (Jurassic) oceanic anoxic event: environmental change and differential subsidence. Sedimentology 55, 1011–1028.
Xu, W., Ruhl, M., Jenkyns, H.C., Leng, M.J., Huggett, J.M., Minisini, D., Ullmann, C.V., Riding, J.B., Weijers, J.W., Storm, M.S., 2018. Evolution of the Toarcian (early Jurassic) carbon-cycle and global climatic controls on local sedimentary processes (Cardigan Bay Basin, UK). Earth Planet. Sci. Lett. 484, 396–411.
Zhao, M.-Y., Zheng, Y.-F., 2014. Marine carbonate records of terrigenous input into Paleotethyan seawater: geochemical constraints from Carboniferous limestones. Geochim. Cosmochim. Acta 141, 508–531.
Zhou, Y., Pogge von Strandmann, P.A.E., Zhu, M., Ling, H., Manning, C., Li, D., He, T., Shields, G.A., 2020. Reconstructing Tonian seawater $^{87}Sr/^{86}Sr$ using calcite microspar. Geology. 48, 462–467.